A multi-proxy lake sediment record of Indian summer monsoon variability during the Holocene in southern India

K. Sandeep [a],[*],[1], R. Shankar [a], Anish Kumar Warrier [a],[2], M.G. Yadava [b], R. Ramesh [b],[3], R.A. Jani [b], Z. Weijian [c], Lu Xuefeng [c]

[a] Department of Marine Geology, Mangalore University, Mangalagangotri-574 199, India
[b] Physical Research Laboratory, Navrangpura, Ahmedabad, Gujarat-380009, India
[c] Xi'an AMS Center, Institute of Earth Environment, Xi'an, China

ARTICLE INFO

ABSTRACT

We present here an 11,000-year palaeomonsoonal record from a sediment core (SS-1) from Shantisagara (SS) Lake in Peninsular India, which is the longest published so far from the region. This is also a region with limited palaeoclimate records. Environmental magnetic, organic geochemical, sedimentological and carbon isotopic studies were carried out on the SS-1 sediments to reconstruct the Indian summer monsoon (ISM) variability during the Holocene. The chronology of the sediments is constrained by three AMS ^{14}C dates. Environmental magnetic data reveal that there is no contribution from bacterial magnetite, greigite and anthropogenic magnetite/ lithogenic grains and that the magnetic signal is contributed mainly by the pedogenic component. The environmental magnetic data also depict variations in pedogenic magnetite production in the catchment and detrital influx to the lake, which in turn is related to monsoonal rainfall amount. The sedimentological data reveal variations in sediment size related to monsoon. The C_{org}/N ratio and δ^{13}C indicate palaeovegetational variations in the SS catchment. Periods of strong monsoon are characterized by high values of concentration-dependent magnetic parameters like χ_{lf}, χ_{fd}, χ_{ARM} and SIRM, high sand content, low C_{org}/N ratio (fully aquatic-deep water conditions), relatively depleted δ^{13}C values (more C_3 but less C_4 land plants) and vice versa. The prominent palaeomonsoon events documented in this study are: (i) 11,100–10,700 cal yr BP with a weak ISM, (ii) 10,700 to 8600 cal yr BP characterized by intensified ISM, corresponding to the Early Holocene Optimum, (iii) 8600 to 4500 cal yr BP with a weakened ISM, (iv) 4500 to 3300 cal yr BP characterized by fluctuating monsoonal conditions, (v) 3300 cal yr BP to the Present with a slight increasing trend in ISM. A similar pattern is also documented in many palaeomonsoon records from the region, which indicate that Shantisagara sediments were able to record regional climatic variations as well.

© 2017 Elsevier B.V. All rights reserved.

1. Introduction

The Indian summer monsoon (ISM; also known as the southwest monsoon) is a vital component of the Asian monsoon system and is the main source of freshwater for people of the Indian sub-continent. During the past few decades, there have been large-scale variations in monsoonal precipitation, leading to excessive floods and severe droughts in different parts of India. This has been largely attributed to global warming (Church and White, 2006; Roxy et al., 2016). There is

a need to study variations of ISM during the geologic past, as it will help in understanding the present changes and model future monsoonal variations. Palaeoarchives, such as marine (Thamban et al., 2007; Kessarkar et al., 2013; Naik et al., 2014; Saraswat et al., 2013, 2016) and lacustrine (Prasad et al., 2014; Rawat et al., 2015a, 2015b) sediments, speleothems (Yadava et al., 2004), and tree-rings (Borgaonkar et al., 2010) have been widely used to reconstruct the ISM variability with different temporal resolution. Although marine sediments provide a long record of palaeomonsoon, their temporal resolution is poor and major climatic events during the Holocene are not well documented except for a few studies (Nigam et al., 1995; Staubwasser et al., 2003). In this regard, lake sediments have the potential of providing high-resolution records of palaeomonsoon. Compared to marine sediments, lake sediments provide direct evidence of the past events on a local or regional scale, with a relatively high temporal resolution. There have been studies on many lake and palaeolake deposits from western India (Prasad et al., 2014), northwestern India (Dixit et al., 2014a,

---

2014b) and the Himalaya (Rawat et al., 2015a, 2015b; Mishra et al., 2015) to reconstruct the ISM variability. However, very few lakes from southern India have been investigated for the reconstruction of Holocene ISM variability (Shankar et al., 2006; Warrier and Shankar, 2009; Warrier et al., 2014; Sandeep et al., 2015; Bhattacharyya et al., 2015, Warrier et al., 2017, Sandeep et al., 2017), most of them providing monsoonal history of only the Late Holocene. Hence, it needs to be verified whether major monsoonal events, reported by many researchers, like the strengthening of ISM during the Early Holocene (Prasad et al., 2014), its weakening after ~7 ka BP (Fleitmann et al., 2007; Demske et al., 2009), dry episodes or abrupt weakening of ISM around 8.2 ka BP and 4.2 ka BP (Staubwasser et al., 2003; Dixit et al., 2014a, 2014b) were widespread phenomena and prevalent in southern India too.

In this study, we have adopted a multi-proxy approach (environmental magnetism, sedimentology, organic geochemistry and carbon isotopes) on the sediments deposited in Shantisagara (hereafter referred to as SS), a large lake located in southern India, to reconstruct the ISM variability during the Holocene.

Environmental magnetism is the systematic study of magnetic properties of soil and sediment samples. Magnetic minerals are ubiquitous and their presence in sediments and soils provides a sensitive medium to record changes in environmental conditions (Evans and Heller, 2003). These minerals may be produced, transported and deposited in different depositional basins. By studying the magnetic mineral concentration, grain-size and mineralogy, it is possible to identify the environmental processes operating in the catchment area. Secondary magnetic minerals also form from iron leached out from parent rocks by chemical processes or biogenic effects (Dearing et al., 1996) near the soil surface during weathering and pedogenesis (Dearing et al., 1997). The secondary magnetic minerals, eroded from the catchment and deposited on lake beds, form the basis of palaeoclimatic reconstruction. The technique has several advantages over others in being easy, rapid, sensitive, and non-destructive.

Down-core variations of particle size in sediments indicate changes in transport energy, lake level and provenance (Conroy et al., 2008). Rainfall plays a crucial role in the transport and deposition of these sediments from the catchment to the lake basin. During periods of high rainfall, the velocity of the transporting medium increases, enhancing the influx of coarse sediments in the lake. During periods of low rainfall, however, fine sediments are carried to deep water regions of the lake, due to the reduction in stream velocity (Chen et al., 2004; Conroy et al., 2008). Hence, sediments containing coarse (fine) particles indicate high (low) rainfall conditions.

Organic matter in sediments originates from the complex mixture of lipids, carbohydrates, proteins, and other biochemicals produced by organisms that live both in the lake and its watershed (Meyers and Ishiwatari, 1993; Meyers and Lallier-Verges, 1999). It provides information about lacustrine palaeoenvironments as the type and abundance of plant life in and around the lake change, as do the composition and amount of the resulting organic matter. The advantage of lacustrine organic proxies is that short-term processes that affect organic matter delivery and burial are amplified in the sediment record because of the high sedimentation rate and high primary productivity in lakes (Meyers, 2003). The C_{org}/N ratio of organic matter may be used to differentiate between organic matter derived from aquatic algae/plankton and that derived from terrestrial plants. The C_{org}/N ratio together with the isotopic signature of organic matter helps to differentiate between contributions from C_3 and C_4 terrestrial plants, which in turn, may be used to infer the climatic conditions of the period during which they lived.

2. Regional setting

2.1. Location, physiography and geology

Shantisagara Lake (Fig. 1) is situated in Channagiri Taluk of Davanagere District, Karnataka State in southern India (14°8′34″N;

75°52′56″E). It is a large lake, covering an area of ~25 sq. km. The average water depth is 5 m. The lake is in its natural setting and receives sediments from the catchment during the SW monsoon. It is not connected to any river network and there are no major industries in the vicinity of the lake. Although human settlements are present near the lake, there are no major pollution or garbage sources and the lake water is clean. Small round boats are used for fishing in the lake. But there are no mechanized boats. Therefore, it is reasonable to assume that the magnetic (and other) properties of Shantisagara (SS) sediments must be a reflection of natural processes only and may be correlatable with the climate of the lake catchment. The western and southern sides of the lake have undulating hills (Fig. 1). They are covered by the Sulekere State Forest. The maximum elevation of the area is about 800 m. The northern and eastern sides are nearly plain and have a relatively low elevation (around 620 m) where small scale agriculture is carried out. The geology of the area is confined to the Chitradurga Group of the Dharwar Super Group and the Peninsular gneissic complex. The main rock types are migmatites and grano-dioritic to tonalitic gneiss belonging to the Peninsular Gneissic Group. Also present are quartz-chlorite schist with orthoquartzite, acid volcanics, greywacke-argillite and basal polymict conglomerate - all belonging to the Chitradurga Group (Geological and Mineral Map of Karnataka and Goa, 1981; Radhakrishna and Vaidyanadhan, 1994). The Lake and the surrounding area are a part of the Shimoga Basin. The soil is mostly reddish brown, clayey loam. Sandy loam is also present in some areas (Karnataka Forest Department, 2003).

2.2. Climate and vegetation

About 80% of the annual rainfall is received during the southwest monsoon from June to September. The rainfall data (1900–2010 CE) for Channagiri Station (India Meteorological Department, 2008; IMD) indicates that the annual rainfall varies from 419 to 1400 mm with an average of 795 mm. There are about 50 rainy days in a year (Karnataka Forest Department, 2003). The mean daily maximum temperature is 35.8 °C and the mean daily minimum temperature 22.2 °C. There is a rapid increase in temperature after January and the hottest month is April. Humidity is high during rainy season and exceeds 60%. The driest period of the year is from January to March when the relative humidity is <35% during daytime. Winds are generally light with some increase in speed during the monsoon (Karnataka Forest Department, 2003). Sulekere and the Bhadrapur State Forests, which belong to the Shantisagara Range, Bhadravati Forest Division, are located in the eastern side of the lake. The vegetation of the area comes under the categories of tropical dry teak-bearing forest and dry deciduous scrubs (Karnataka Forest Department, 2003).

3. Materials and methods

3.1. Materials

A 1.3-m sediment core (SS-1) from Shantisagara was collected in November 2007 by pushing a PVC pipe (diameter: 1.5 in.; water depth = 5 m) into the sediment column. In order to obtain high-resolution data, the core was sub-sampled at intervals of 0.5 cm. The sub-samples were stored in plastic bags. Environmental magnetic analysis was carried out for all the sub-samples (n = 264), whereas organic geochemical (n = 20), carbon isotopic (n = 20), particle size (n = 23) and ^{14}C studies (n = 3) were carried out on selected sub-samples. Samples of surface (n = 10) and sub-surface (n = 23) soils from the lake catchment were also collected (Fig. 1b). The details of soil samples and sampling methods are provided by Sandeep et al. (2012).
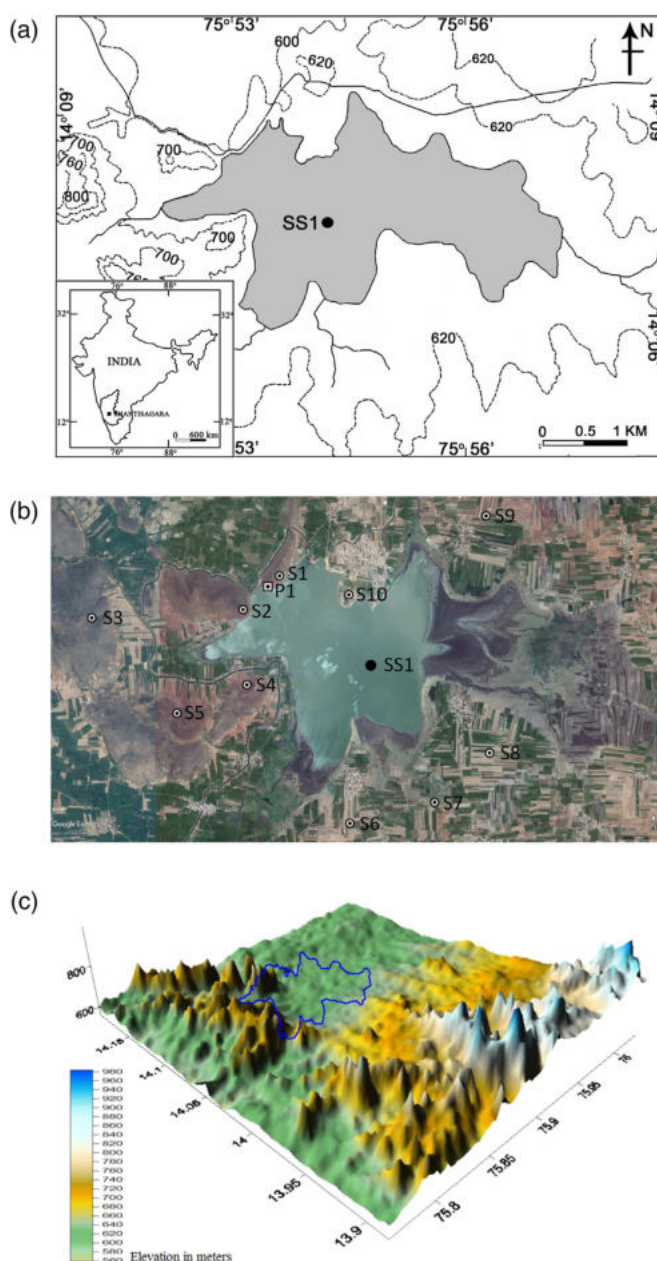
Fig. 1. (a) Topographic map of Shantisagara Lake and surrounding areas (Source: Survey of India Toposheet Number 48 N/16). Contours are in meters. Inset map shows the location of the lake in southern India. SS-1 is the core location; (b) Satellite image of Shantisagara Lake and surrounding areas along with the core location (Source: Google Earth) (SS1 = core location; S1-S10 = location of surface soil samples from the lake catchment; P1 = location of sub-surface soil samples); (c) Digital Elevation Model (DEM) of Shantisagara Lake (blue outline) and surrounding areas. Undulating hills are present to the west and south of the lake. (For interpretation of the references to colour in this figure legend, the reader is referred to the web version of this article.)

3.2. Methodology

3.2.1. AMS ^{14}C dating

Carbon-14 dating by accelerator mass spectrometry was carried out on the organic matter of bulk sediment samples from selected depths (Table 1) at the Xi'an Accelerator Mass Spectrometer Center, Institute of Earth Environment, CAS, China. The ^{14}C ages were calibrated using the code *clam* (Version 2.2; Blaauw, 2010) which runs on the open source software 'R' (Version 3.3.2; R Development Core Team, 2013) and uses IntCal13.14C radiocarbon calibration data (Reimer et al., 2013). An age-depth model (Fig. 2) was constructed by linear interpolation model. Sedimentation rate was calculated from the age-depth

model. The R code of *clam* calculates the confidence intervals for undated levels from the calibrated age distribution (at 95% interval) of every dated depth and the age-model is drawn through these models and the calibrated age calculated (Blaauw, 2010) for every depth.

3.2.2. Environmental magnetic measurements

Environmental magnetic properties of sediment samples were measured using standard rock magnetic methods (Walden et al., 1999). Low- (0.47 kHz; χ_{lf}) and high- (4.7 kHz; χ_{hf}) frequency magnetic susceptibility were measured on a Bartington Susceptibility Meter (Model MS2B) with a dual-frequency sensor. A Fe_3O_4 (1%) standard was used to calibrate the sensor. Using the χ_{lf} and χ_{hf} values, the percentage

Table 1
AMS ^{14}C dates on bulk organic matter from the Shantisagara Lake sediment core SS-1.

Sample no.	Xi'an Lab ID	Depth (cm)	^{14}C age (yr BP)	δ^{13}C (‰)	Weighted mean of calibrated age (years)	Calibrated age 2-σ (cal yr BP)
SSA1	XA3002	54–55	3420 ± 30	− 15.85 ± 0.47	3669	3818–3581
SSA2	XA3339	93–94	9100 ± 30	− 23.21 ± 0.22	10,247	10,369–10,199
SSA3	XA3340	122–123	9540 ± 40	− 23.83 ± 0.22	10,902	11,081–10,709

Note: The AMS ^{14}C dates were calibrated using the code *clam* (Version 2.2; Blaauw, 2010), which runs on the open source software 'R' (Version 3.3.2; R Development Core Team, 2013) and uses the IntCal13.14C radiocarbon calibration data (Reimer et al., 2013).

frequency-dependent susceptibility (χ_{fd} %) was calculated by using the formula, χ_{fd} % = (($\chi_{lf} - \chi_{hf}$) / χ_{lf}) × 100 (Dearing, 1999a). Anhysteretic remanent magnetisation (ARM) was induced in the samples using a Molspin AF demagnetiser (with an ARM attachment) set with a peak alternating field of 100 milli Tesla (mT) and a DC biasing field of 0.04 mT. The ARM induced was measured on a Molspin spinner fluxgate magnetometer. The susceptibility of ARM (χ_{ARM}) was calculated by dividing the mass-specific ARM by the size of the biasing field (0.04 mT = 31.84 Am^{-1}; Walden, 1999). Isothermal remanent magnetisation (IRM) was induced in the samples at increasing field strengths (20, 60, 100, 300, 500 and 1000 mT) using a Molspin pulse magnetiser and the remanence acquired measured using the Molspin spinner fluxgate magnetometer. The isothermal remanence induced at 1 T field (the maximum field attainable in the Environmental Magnetism Laboratory, Mangalore University) was considered as the saturation isothermal remanent magnetisation (SIRM). The sediment samples were oven-dried at 35 °C and the dry sample weight was used to calculate the magnetic parameter values on a mass-specific basis. To determine the magnetic grain size and mineralogy of magnetic minerals, inter-parametric ratios like χ_{ARM}/SIRM, χ_{ARM}/χ_{lf}, χ_{ARM}/χ_{fd}, SIRM/χ_{lf}, and S-ratio, and HIRM were calculated (Maher et al., 1999; Walden, 1999; Evans and Heller, 2003). The S-ratio used in this study involved not the classical IRM$_{-300mT}$ (Thompson and Oldfield, 1986) but the forward field IRM$_{300mT}$ (Bloemendal et al., 1992; Heslop, 2009). Similarly, forward field IRM$_{300mT}$ was used for calculating HIRM (Maher et al., 1999).

Fig. 2. Age-depth model for the Shantisagara sediment core (SS-1). It was constructed with the linear interpolation model using the weighted mean of probability distribution of calibrated ^{14}C ages by 'R' code of *clam* (Version 2.2; Blaauw, 2010). The sedimentation rate is given for each interval. The 2σ probability range of calibrated dates is shown in black and that of interpolated ages in grey. The black line is the best age-depth model drawn through the weighted means of all the calendar ages.
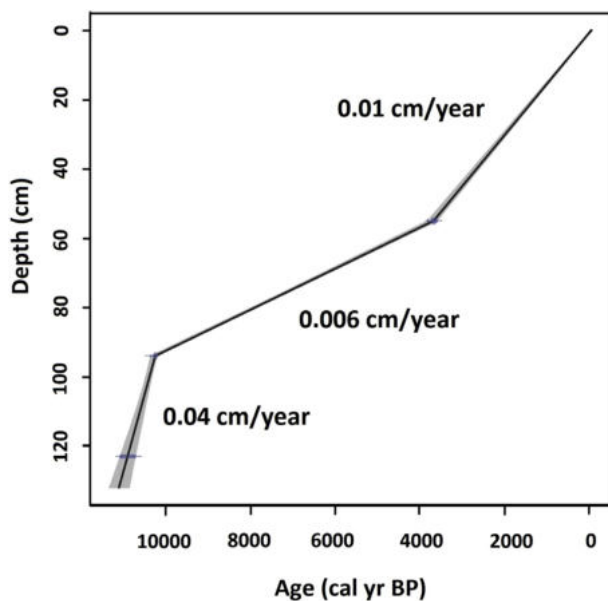
3.2.3. Particle size analysis

Particle size analysis was carried out on 23 sub-samples. About 4 g of each sediment sample was used for the analysis. The organic matter and carbonate contents were removed by treating the samples with 30% H_2O_2 and 10% acetic acid respectively. The sand fraction was separated by wet-sieving through an ASTM test sieve no. 230 (62 μm pore diameter). After removal of sand, the silt + clay fraction was transferred to a 1000 ml measuring cylinder. 1 g of sodium hexametaphosphate was added to prevent flocculation. After making it up to 1000 ml volume, the silt and clay fractions were determined using pipette analysis (Carver, 1971). The column containing silt and clay was stirred vigorously for about 1 min using a long stirring rod. After 20 s of stoppage of stirring, 20 ml of the liquid was pipetted out from 20 cm depth that contains the silt + clay fraction. After 3 h 10 min, 20 ml of the liquid was pipetted out from 5 cm depth that contains only the clay fraction. The total weight of the clay fraction was calculated by multiplying the weight of clay by 50. A value of 1 g was subtracted from the value obtained to account for the weight of sodium hexametaphosphate. Similarly, the total weight of the silt + clay fraction was also calculated. From these values, the total weight of the silt fraction was determined. The three fractions (sand, silt and clay) are expressed as percentages.

3.2.4. Organic geochemistry

Organic geochemistry (C, N, $CaCO_3$ and δ^{13}C) was determined for 20 samples. Bulk sediment samples were dried in a hot air oven at 40 °C and finely ground and homogenized using an agate mortar and pestle. About 2 g of the sediment sample was taken in a beaker and 1 N dilute HCl added in small increments until effervescence stopped (Schumacher, 2002). It was kept overnight at room temperature to facilitate complete removal of carbonates. The sample was washed 3–4 times with deionised water and dried in the hot air oven at 100 °C. Weight loss after the HCl treatment gives the weight of $CaCO_3$ or inorganic carbon and is expressed as percentage (error ≤ 0.5%). The organic carbon and nitrogen in the decarbonated samples were determined using a CHNS analyzer (Model: Elementar Vario EL III; error ≤ 0.1%) at the Sophisticated Test and Instrumentation Centre, Cochin University of Science and Technology, Kochi. From the carbon and nitrogen percentages, C_{org}/N ratio was calculated and expressed as atomic ratio, which is obtained by multiplying the mass ratio with 1.167 (Meyers and Terranes, 2001).

3.2.5. Carbon isotopic analysis

To determine the δ^{13}C of organic carbon, a small quantity (~1 g) of sediment sample was treated with 10% HCl for several hours, dried and heated at 900 °C along with CuO powder and silver foil (Northfelt et al., 1981). The CO_2 evolved was purified cryogenically before injecting it into the mass spectrometer. The isotopic composition is expressed as δ^{13}C in parts per thousand (‰) relative to the Vienna-Pee Dee Belemnite (V-PDB) standard. ($\delta = ((R_{sam}) - (R_{std}) - 1) \times 1000$ where R_{sam} and R_{std} refer to the ^{13}C/^{12}C ratio in the sample and the standard respectively). The external precision for the laboratory standard was ± 0.12‰ for δ^{13}C (Yadava and Ramesh, 1999). For reproducibility check, a few replicates were run and they revealed no significant differences. The conversion of organic carbon to CO_2 gas and the subsequent δ^{13}C analysis using an isotope ratio mass spectrometer (Model: PDZ Europa
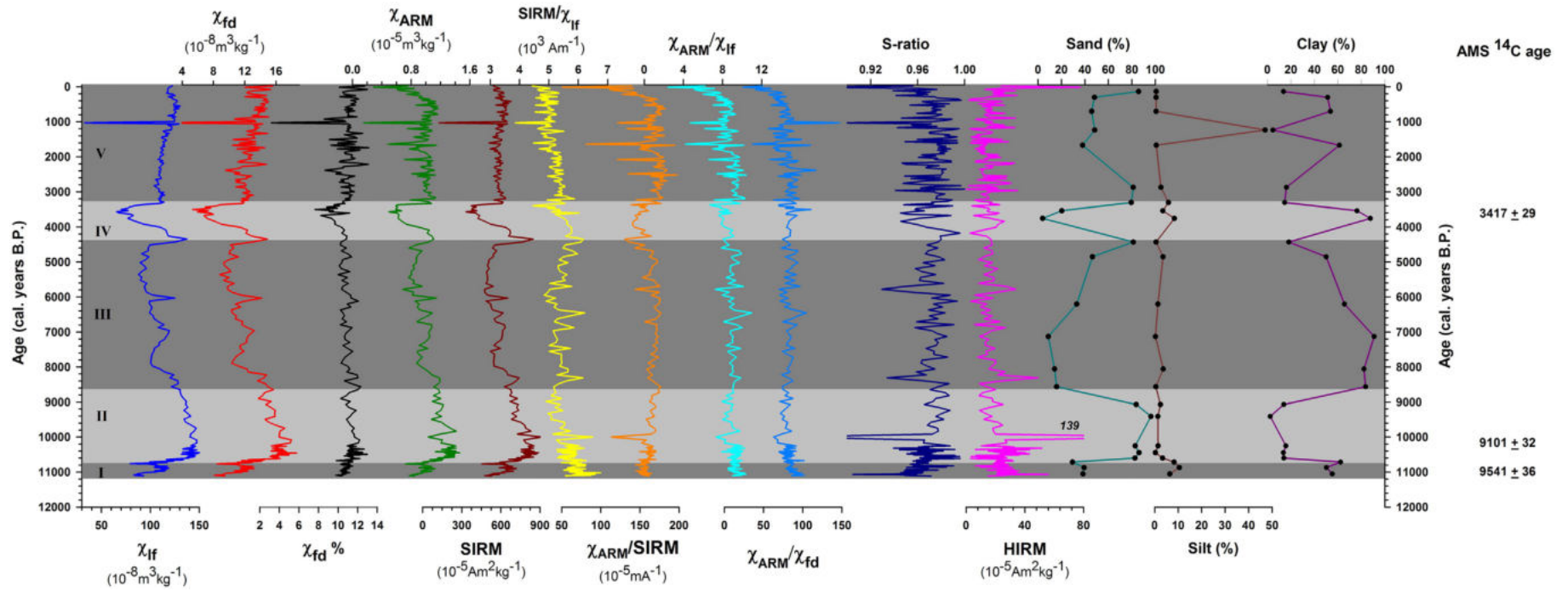
Fig. 3. Down-core variations of rock magnetic and particle size data for Shantisagara sediment core (SS-1). The entire record may be broadly divided into five zones or periods based on multi-proxy data.

GEO20–20) were carried out at the Physical Research Laboratory, Ahmedabad.

4. Results

4.1. Chronology

The chronology of the sediment core is constrained by three AMS ^{14}C dates. The calibrated age ranges at 95% confidence interval (2σ) and their weighted means are given in Table 1. The limited number of C-14 dates on the core and the uncertainties in chronology due to reservoir effect are lacunas in our study. Sedimentation rate varies from 0.04 cm/year to 0.006 cm/year (Fig. 2). The average sedimentation rate is 0.019 cm/year, so that the 1.32 m core represents the past ~ 11,100 cal yr BP. Although the sediment core was sub-sampled at 0.5 cm interval, the record is yet not of high temporal resolution because of the low sedimentation rate. A possible reason for this is that being located in a low-rainfall area (average annual rainfall = 795 mm; IMD), sediment delivery to SS may be low. Besides, the sediment delivered gets deposited over a large area (~25 km^2) of Shantisagara, resulting in a low sedimentation rate. Nevertheless, it covers the entire Holocene. Even with the low temporal resolution, therefore, it has the potential to reveal broad long-term trends in rainfall over the entire Holocene in southern India.

### 4.2. Environmental magnetic properties of SS-1 sediments

Environmental magnetic parameters showing the magnetic concentration, grain-size and mineralogy for core SS-1 are plotted against age in Fig. 3. Magnetic susceptibility (χ_{lf}) indicates the total concentration of magnetic minerals present in a natural sample (Walden et al., 1999). The χ_{lf} values during the Holocene vary between 32.85×10^{-8} m^3 kg^{-1} (16 cm; 1027 cal yr BP) and 150.59×10^{-8} m^3 kg^{-1} (102.5 cm; 10,439 cal yr BP) with an average of 114.81×10^{-8} m^{3}kg^{-1}. The high χ_{lf} values throughout the core indicate that the magnetic signal recorded in SS-1 is primarily due to ferrimagnetic minerals, with little contribution from canted antiferromagnetic, paramagnetic and diamagnetic minerals (Thompson and Oldfield, 1986; Walden et al., 1999). Percent frequency-dependent susceptibility (χ_{fd} %) indicates the proportion of superparamagnetic (SP) grains (Dearing, 1999a). The formation of SP grains is mainly due to pedogenesis or fire activity (Evans and Heller, 2003; Oldfield and Crowther, 2007). The χ_{fd} % values for the SS-1 sediments vary from 3.18% (16 cm; 1027 cal yr BP) to 13.1% (26.5 cm; 1738 cal yr BP; Fig. 3). The average χ_{fd} % value is 10.93%. Such high values suggest that the samples have a high content of SP and fine grained magnetic minerals (Dearing, 1999a). The susceptibility of anhysteretic remanent magnetization (χ_{ARM}) is biased towards magnetic minerals of stable single domain (SSD) grain size (Maher, 1988). Values of χ_{ARM} vary between 0.15×10^{-5} m^3 kg^{-1} (16 cm; 1027 cal yr BP) and 1.46×10^{-5} m^3 kg^{-1} (102.5 cm; 10,439 cal yr BP) with an average of 1.01×10^{-5}m^{3}kg^{-1}. Saturation isothermal remanent magnetization (SIRM) is generally influenced by the concentration of all remanence-carrying magnetic minerals (Walden, 1999) and, hence, reflects the total magnetic mineral content (Oldfield, 1991). Values of SIRM range between 126.66×10^{-5} Am^2 kg^{-1} (16 cm; 1027 cal yr BP) and 911.97×10^{-5} Am^2 kg^{-1} (92.5 cm; 9994 cal yr BP) with an average of 622.6×10^{-5} Am^2 kg^{-1}, suggesting a high concentration of magnetic minerals during the Holocene.

S-ratio (IRM$_{300mT}$/IRM$_{1000mT}$) is indicative of the relative proportions of ferrimagnetic and antiferromagnetic minerals in the sample (Walden et al., 1999; Evans and Heller, 2003). An S-ratio value close to unity denotes the dominance of magnetically "soft" minerals like magnetite and maghemite whereas significantly low values indicate the dominance of magnetically "hard" minerals like hematite and goethite. Values of S-ratio in SS-1 are extremely high and fluctuate between 0.85 and 1.00 (Fig. 3), indicating the dominance of low-coercivity, magnetically "soft" minerals like magnetite and maghemite. This supports the fact that the magnetic mineralogy of SS-1 sediments is dominated by ferrimagnetic minerals like magnetite and maghemite. The presence of canted antiferromagnetic minerals like hematite in the samples is also evident from HIRM values (Fig. 3). The HIRM values fluctuate between a low of 0.10×10^{-5} Am^2 kg^{-1} (44 cm; 2924 cal yr BP) and a high of 134.87×10^{-5} Am^2 kg^{-1} (92.5 cm; 9994 cal yr BP) with an average of 19.35×10^{-5} Am^2 kg^{-1}, suggesting the presence of high-coercivity magnetic minerals like hematite in SS-1.

Inter-parametric ratios, χ_{ARM}/SIRM and χ_{ARM}/χ_{lf}, are used to determine the magnetic grain size. High ratio values generally indicate a fine magnetic grain size and vice versa (Oldfield, 1991). Both the ratio values exhibit similar down-core variations as also evident from a statistically significant correlation between them ($r^2 = 0.57$; n = 262; p < 0.0001). The χ_{lf} vs. χ_{fd} % biplot (Fig. 4a) gives a fair indication of the presence of SP magnetic grains, which control the magnetic susceptibility signal in the sediment core. This is further corroborated by the χ_{ARM} vs. χ_{lf} biplot (Fig. 4b; also known as the King's Plot), which is used to estimate the concentration and grain size of magnetic minerals (King et al., 1982; Bloemendal et al., 2003). The SS-1 sediments have a high
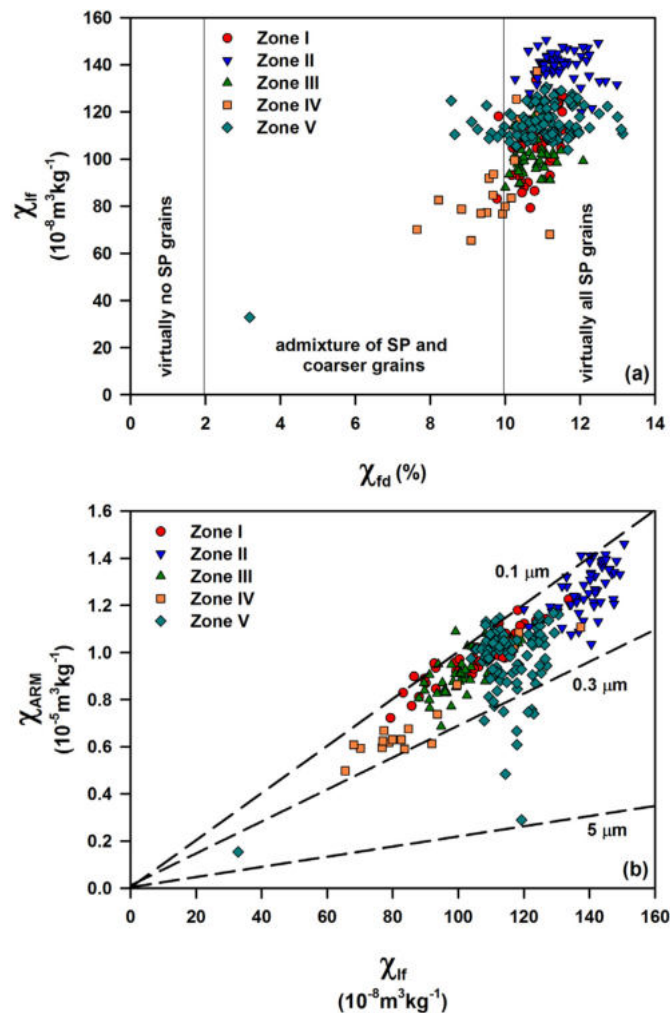
Fig. 4. (a) Biplot of χ_{lf} vs. χ_{fd} % for SS-1 sediment samples. Note that χ_{fd} % values >10 indicate fine-grained magnetic minerals and with a high proportion of SP magnetic grains; (b) Biplot of χ_{lf} vs. χ_{ARM} (King et al., 1982) for SS-1 sediments. The data show fine-grained magnetic minerals in the size range of 0.1-0.3 μm.
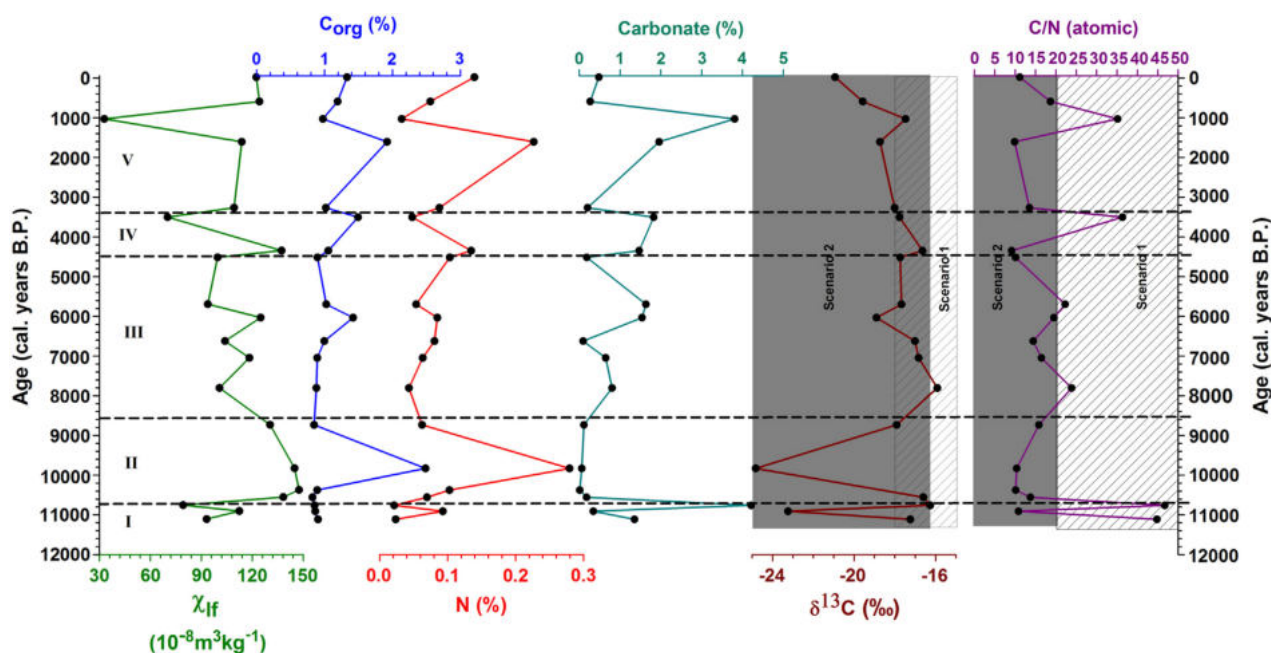
Fig. 5. Down-core variations of magnetic susceptibility (χ_{lf}), carbonate %, organic carbon (C_{org}), nitrogen, C/N ratio and $\delta^{13}C$ for selected samples of Shantisagara sediments. *Note*: C_{org} does not exhibit any significant relationship with χ_{lf}, whereas N content exhibits a positive correlation. Carbonate and C/N ratio exhibit a high negative correlation with χ_{lf}. Although $\delta^{13}C$ also exhibits a negative correlation, it is not statistically significant (r = -0.36). The five climatic phases are shown using broken lines. The two scenarios based on C/N ratio and $\delta^{13}C$ values are also displayed (for details see text).

concentration of magnetic minerals and are predominantly fine-grained (0.1–0.3 μm; Fig. 4b).

4.3. Particle size data

The three particle size classes (sand, silt and clay) in Shantisagara sediment samples exhibit considerable down-core variations (Fig. 3). The sand and clay contents range from 4 to 96.2% and from 2.4 to 90.8% respectively. The silt content is relatively low (0.3 to 11.2%). The sand percentage exhibits a significant positive correlation of 0.68 with χ_{lf} (n = 23; p < 0.01) and 0.62 with χ_{fd} (n = 23; p < 0.01). It also shows positive correlations with χ_{ARM} (r = 0.50; n = 23; p < 0.01) and SIRM (r = 0.66; n = 23; p < 0.01). By contrast, clay percentage exhibits a negative correlation of −0.65 and −0.58 with χ_{lf} and χ_{fd} respectively (n = 23; p < 0.01). It is negatively correlated with χ_{ARM} (r = −0.46; n = 23; p = 0.03) and SIRM (r = −0.63; n = 23; p < 0.01) as well. In fact, sand and clay abundances mirror each other in the sediment core (r = −0.99, p = 0.01; n = 23). Silt content also exhibits a negative correlation with magnetic parameters. For *e.g.*, −0.42 with χ_{lf} (n = 23, p = 0.05) and −0.45 with χ_{fd} (n = 23; p = 0.03). The changes in sand and clay abundances are probably related to rainfall variations. During periods of high (low) rainfall, a large (small) proportion of coarse sediments are transported to the centre of the lake due to the high (low) energy of the transporting medium (Chen et al., 2004; Conroy et al., 2008). This is substantiated by the strong positive correlation of χ_{lf} with sand % and the negative correlation with clay %. Hence, periods characterized by high χ_{lf}, high sand content and low clay percentage experienced high-rainfall conditions and *vice versa* (Fig. 3).

4.4. Organic geochemical, CaCO₃ and carbon isotopic data

Figure 5 depicts the down-core variations of χ_{lf}, CaCO₃, organic carbon, nitrogen, C_{org}/N ratio and $\delta^{13}C$. Carbonate content ranges from 0.01 to 4.2%. Organic carbon content varies between 0.80 and 2.50% whereas nitrogen content ranges between 0.02 and 0.28%. There is no

systematic decrease of nitrogen content with age (Fig. 5). Also, there is a high positive correlation ($r^2 = 0.67$; n = 20, p < 0.001) between the organic carbon and nitrogen contents (Fig. 6a), suggesting that they are organically bound and their losses are due to decomposition of the organic matter. Organic carbon content does not exhibit any significant positive correlation with χ_{lf} whereas N content does (r = 0.53; p = 0.01, n = 20). The atomic C_{org}/N ratio values vary from 9.1 to 46.7 with an average of 19.6 and exhibit a high negative correlation with χ_{lf} (r = −0.72; p < 0.001; n = 20). The $\delta^{13}C$ of organic matter varies from −24.8 to −15.9‰ (Fig. 5).

5. Discussion

5.1. Origin of magnetic minerals in Shantisagara sediments

Sediments contain magnetic minerals, which may be derived from different sources (Walden et al., 1999). Apart from detrital input, there may be contributions from bacterial magnetite (Snowball, 1994), authigenic greigite (Snowball, 1991) and anthropogenic magnetite derived from industrial activity, vehicular emissions, *etc.* (Gautam et al., 2004). Besides, there is also the possibility of diagenetic dissolution of magnetic minerals due to the decomposition of organic matter (Anderson and Rippey, 1988). Data for SS-1 sediment and catchment soil samples were plotted in the χ_{ARM}/χ_{lf} *vs.* χ_{ARM}/χ_{fd} diagram of Oldfield (2007) to examine if bacterial magnetite contributes to the magnetic signal (Fig. 7a). The sediment and soil samples plot in the envelope for soil, palaeosol and catchment-derived fine sediments. They exhibit considerably low ratio compared to the threshold values ($\chi_{ARM}/\chi_{lf} < 40$ and $\chi_{ARM}/\chi_{fd} < 1000$; Dearing, 1999b) reported for bacterial magnetite. Hence, the presence of bacterial magnetite in the samples is ruled out. The SIRM/χ_{lf} ratio for Shantisagara core sediment samples ranges from 3.9 to 6.8×10^3 Am⁻¹ (Fig. 3), which is considerably below the threshold value for greigite (40×10^3 Am⁻¹; Snowball, 1991). Hence, the presence of this iron sulphide mineral too may be ruled out. The down-core trends of inter-parametric ratios (indicative

of magnetic grain size) - χ_{ARM}/χ_{lf}, χ_{ARM}/χ_{fd} and χ_{ARM}/SIRM - (Fig. 3) do not exhibit any steep and simultaneous decrease. Therefore, it appears that magnetic dissolution has not affected the SS-1 magnetic record. The semi-quantitative magnetic granulometry plot of χ_{ARM}/SIRM vs. χ_{fd} % (Dearing et al., 1997) was used to check the presence of anthropogenic/lithogenic magnetic minerals (Fig. 7b). Most sediment samples plot in the SSD/SP transition range whereas surface and sub-surface soil samples do so in the coarse to fine SSD region. None of them plot in the MD + PSD grain size range, which is characteristic of magnetite that is anthropogenic (Gautam et al., 2004) or lithogenic (Maher and Thompson, 1992). The parameter χ_{fd}, which is proportional to the concentration of the superparamagnetic pedogenic component, exhibits a high correlation with χ_{lf} (r = 0.95, p < 0.001, n = 262), confirming the pedogenic origin of magnetite. The data presented above suggest that there are no contributions from bacterial/anthropogenic magnetite and greigite to the SS-1 magnetic record nor is there any dissolution effect that could obliterate the magnetic record. Hence, it may be inferred that the magnetic signal is principally catchment-derived. The magnetically enhanced top-soil from the catchment is eroded, transported and deposited in SS. A magnetic grain size "sorting" is apparent from Fig. 7b. Catchment soils have a wide range of magnetic grain size (MD & PSD to

SSD/SP transition), but what is transported to SS is material of fine magnetic grain size (95% of the samples in the SSD/SP transition range).

5.2. The magneto-climatic record of Shantisagara Lake sediments

The down-core variations of environmental magnetic parameters of the Shantisagara sediment core are shown in Fig. 3. They exhibit considerable fluctuations during the past 11,100 years. The trends of parameters, χ_{lf}, χ_{fd}, χ_{ARM}, SIRM, are nearly similar. High values for these parameters indicate high-rainfall conditions and vice versa. During the ~11,100 to 10,700 cal yr BP period, concentration-dependent parameters exhibit notably low values. However, the values are the highest during the ~10,700 to 8600 cal yr BP period. From ~8600 to 4500 cal yr BP, the values are again low save for two peaks. Fluctuations in the values are documented between ~4500 and 3300 cal yr BP. From ~3300 cal yr BP to the present, the parameters do not exhibit much fluctuation but a slight increasing trend may be discerned.

The concentration-dependent parameters exhibit considerably high correlations with χ_{lf} as evident by their similar trends (Fig. 3). The grain size-dependent parameters, χ_{ARM}/SIRM and χ_{ARM}/χ_{lf}, do not exhibit any noteworthy long-term trends although short-term fluctuations are noted. Values of χ_{lf} do not exhibit any significant correlation with these two ratios (r = 0.10 and 0.08 respectively). On a close scrutiny of the χ_{ARM}/SIRM trend, it is possible to note only subtle differences: Relatively high ratio values (= relatively fine magnetic grain size) correspond to relatively high χ_{lf} values and vice versa. Hence, there is not much variation in magnetic grain size, suggesting that the climate of this region did not leave a strong imprint on magnetic grain size.

Magnetic mineralogy is mainly "soft" as indicated by the high S-ratio values (0.85 to 1.00). Although there are minor fluctuations, there is no long-term trend exhibited by S-ratio. Similarly, HIRM also exhibits short-term fluctuations. Besides, there are no specific periods characterized by increased contribution from magnetically "hard" minerals.

5.3. Holocene record of palaeovegetation variations in the Shantisagara catchment

High carbonate content is indicative of low rainfall or arid climatic conditions and vice versa (Chen et al., 2002; Warrier and Shankar, 2009). This appears to be the case in SS sediments as well: χ_{lf} and carbonate content are negatively correlated (r = −0.72, p < 0.001, n = 20). Low C_{org}/N ratio values indicate deep water conditions in SS because of the predominance of aquatic plankton. Hence, a warm and wet climate may be inferred. A high C_{org}/N ratio hints at a decreased contribution from plankton and shallow water conditions; hence, low rainfall may be discerned (Meyers and Lallier-Verges, 1999; Rühland et al., 2009). This is further exemplified by the fact that there is no significant correlation between C_{org}/N and C_{org}%, indicating that the increase (decrease) in C_{org}/N ratio is not due to high (low) terrigenous influx but due to a relative decrease (increase) in autochthonous contribution by plankton. Hence, there was an increased in wash of soil nutrients during high-rainfall periods (Meyers and Lallier-Verges, 1999), resulting in increased aquatic productivity and low C_{org}/N ratio and vice versa. Stable carbon isotopic composition ($\delta^{13}C$) of organic matter in lakes depends on the dominance of its sources, either land derived or in-situ. It has characteristic values for the type of terrestrial vegetation: ~ −22 to −27‰ for C_3 type pathway and −8 to −13‰ for C_4 type (Fig. 6a). Algae growing in freshwater lakes such as 'SS' use dissolved CO_2 during photosynthesis, which is in isotopic equilibrium with atmospheric CO_2. Therefore, $\delta^{13}C$ values of algae may be indistinguishable from those of terrestrial organic matter from the catchment (Meyers, 2003). However, sources of organic matter in lake sediments may be better deciphered using the additional data of C_{org}/N ratio in a C_{org}/N ratio vs. $\delta^{13}C$ plot (Fig. 6b). Based on the C_{org}/N ratio and carbon isotopic data of SS-1 sediments, two scenarios of climatic conditions may be inferred.
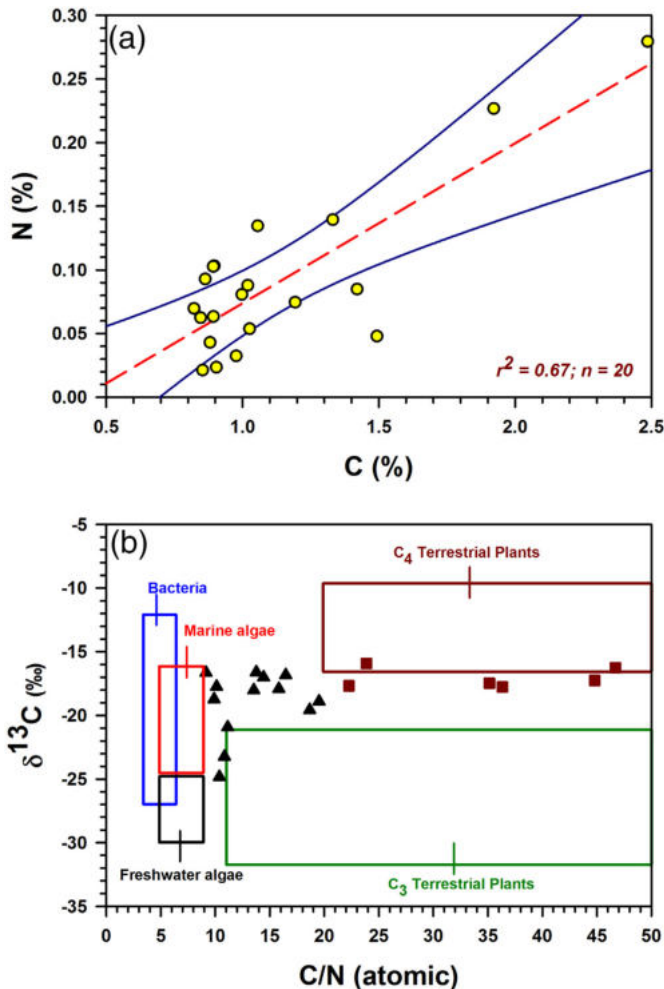

Fig. 6. (a) C vs. N biplot for SS-1 sediment samples. The high correlation between the two parameters indicates that they are organically bound; (b) C/N ratio and organic $\delta^{13}C$ values for bacteria, marine and freshwater planktonic algae and C_3 and C_4 terrestrial plants (after Lamb et al., 2006). Data for Shantisagara Lake sediment samples are shown. The two scenarios described in the text are shown using different symbols. (■ = Scenario 1: C/N ratio > 20 and $\delta^{13}C$ −18 to −15‰ ▲ = Scenario 2: C/N ratio < 20 and $\delta^{13}C$ −25 to −16‰).
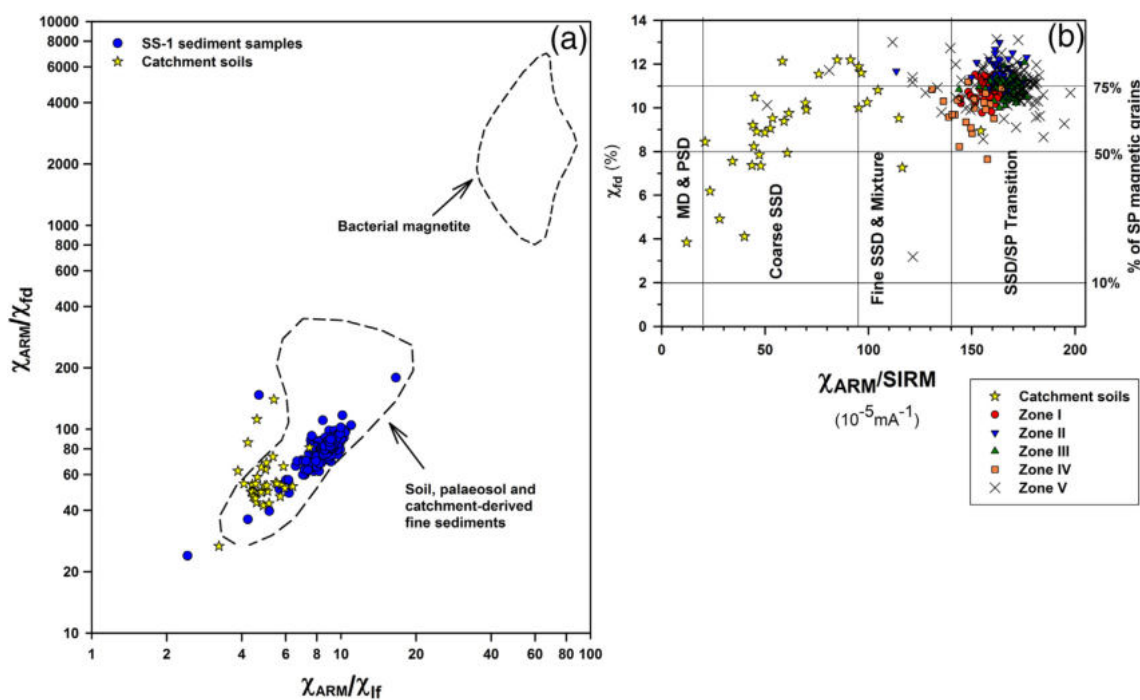
Fig. 7. (a) Bi-logarithmic plot of χ_{ARM}/χ_{lf} versus χ_{ARM}/χ_{fd} (Oldfield, 1994, 2007) for Shantisagara sediments and catchment soils (Sandeep et al., 2012). Note that samples with bacterial magnetite plot near the top right corner with high values for both the ratios (> 40 and > 1000 respectively). Shantisagara sediments and catchment soils plot in a separate envelope with considerably lower values for the two ratios, confirming the absence of bacterial magnetite; (b) Semi-quantitative magnetic granulometry biplot of $\chi_{ARM}/SIRM$ vs. χ_{fd} % (after Dearing et al., 1997 and Maher and Taylor, 1988), with data for the five zones of Shantisagara Lake sediments and catchment soils. Note that most of the sediment samples plot in the SSD/SP transition range, indicating the absence of MD+PSD grains that are suggestive of anthropogenic/lithogenic origin. Catchment soil samples exhibit a coarser grain size (coarse to fine SSD) compared to sediment samples.

Scenario 1: C_{org}/N ratio > 20 and $\delta^{13}C$ − 18 to − 15‰:- High C_{org}/N ratio values may indicate a total absence of plankton due to shrinkage of lake area and low water level. Carbon isotopic values are close to those characteristic of C4 terrestrial plants. These features indicate arid climatic conditions.

Scenario 2: C_{org}/N ratio < 20 and $\delta^{13}C$ − 25 to − 16‰:- Relatively high rainfall conditions and increased water levels are indicated by the presence of aquatics. More negative carbon isotopic values indicate a high proportion of C3 terrestrial plants and high rainfall conditions, whereas less negative or enriched $\delta^{13}C$ values suggest a high proportion of C4 terrestrial plants and low-rainfall conditions. But overall, rainfall is high compared to Scenario 1.

5.4. The palaeoclimate/palaeoenvironment around Shantisagara Lake – A summary based on multiple proxies

The palaeoclimate/palaeoenvironment of the Shantisagara Lake area during the past 11,100 cal yr BP is reconstructed based on various proxies like environmental magnetism, sedimentology, organic geochemistry and carbon isotopes. The Holocene climate was earlier considered to be relatively stable (Lowe and Walker, 2014; Grootes et al., 1993; Dansgaard et al., 1993). However, later studies indicated variability in Holocene climate (Mayewski et al., 2004; Wanner et al., 2008, 2014). This is also reflected in the SS record with low- and high-rainfall intervals. These intervals are delineated based mainly on magnetic parameters, but well supported by other proxies. The major climatic periods witnessed by the Shantisagara area are outlined below.

I. ~11,100 to 10,700 cal yr BP

The concentration-dependent parameters, χ_{lf}, χ_{ARM} and SIRM, exhibit low values during this period. Their average values are 103.3 $\times 10^{-8}$ m^3 kg^{-1}, 0.96 $\times 10^{-5}$ m^3 kg^{-1} and 614.9 $\times 10^{-5}$ Am^2 kg^{-1} respectively. Prior to 11,000 cal yr BP, the values are remarkably low (average values being 89.1 $\times 10^{-8}$ m^3 kg^{-1}, 0.87 $\times 10^{-5}$ m^3 kg^{-1} and 548.3 $\times 10^{-5}$ Am^2 kg^{-1} respectively). The lowest values are recorded at ~10,700 cal yr BP. Pedogenesis was weak during this period as indicated by the relatively low χ_{fd} values (8.1 to 13.1 $\times 10^{-8}$ m^3 kg^{-1}; average = 11.1 $\times 10^{-8}$ m^3 kg^{-1}) whose trend is similar to those of other concentration-dependent parameters. S-ratio also exhibits relatively low values, ranging from 0.9 to 0.99. On the other hand, HIRM expectedly exhibits an opposite trend, with relatively high values (6.3 to 56.0 $\times 10^{-5}$ Am^2 kg^{-1}). After 10,700 cal yr BP, there is a rapid increase in the concentration-dependent parameters up to 10,700 cal yr BP.

The carbonate % is relatively high during this period and varies from 0.34 to 4.22% (average = 1.97%). The C_{org}/N ratio varies from 10.8 to 46.7 (average = 29.2). Two samples from this period exhibit high C_{org}/N values of 44.8 and 46.7, whereas one sample (with a slightly higher χ_{lf}) has a low C_{org}/N value. Such high C_{org}/N ratio values indicate the complete absence of plankton, implying a low water level or even drying up of the lake. The C_{org} content ranges from 0.85 to 0.90% and N content from 0.02 to 0.09%. The $\delta^{13}C$ values range from − 16.3 to − 23.2‰ (average = − 18.9‰). One sample with a slightly higher χ_{lf} exhibits a more depleted $\delta^{13}C$ value of − 23.2‰. Except the time represented by this sample, the period is characterized by a high proportion of C4 plants (Scenario 1).

The various lines of evidence presented above suggest that rainfall was generally low during ~11,100 to 10,700 cal yr BP before the advent
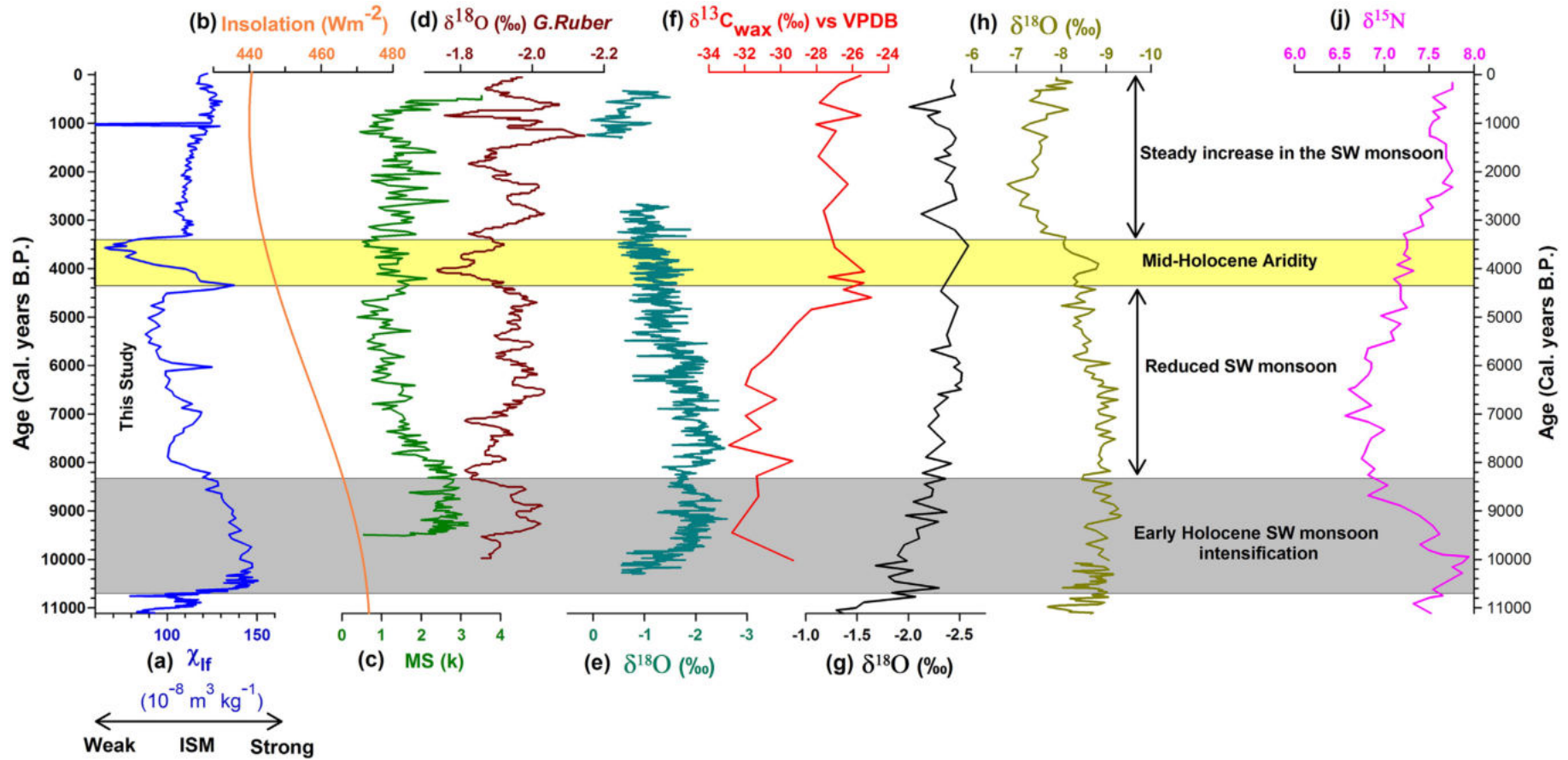
Fig. 8. Comparison of (a) Shantisagara χ_{lf} record with: (b) insolation data (14°N, June 21; Laskar, 1990); (c) Magnetic susceptibility (k) of core SK 148/55 collected from the western continental margin of India (Thamban et al., 2007); (d) $\delta^{18}O$ of *G. ruber* from sediments off the Sindhu (Indus) River mouth (Staubwasser et al., 2003); (e) $\delta^{18}O$ of stalagmite (Q5) from Oman (Fleitmann et al., 2003); (f) $\delta^{13}C_{wax}$ record from Lonar Lake sediments (Sarkar et al., 2015); (g) $\delta^{18}O$ record from marine sediments (Saraswat et al., 2016); (h) $\delta^{18}O$ record of a stalagmite from Dongge Cave, China (Dykoski et al., 2005); and (i) $\delta^{15}N$ record from a sediment core off Oman (Altabet et al., 2002).

of the Holocene. However, the monsoon had rapidly strengthened during the latter half of this period.

II. *~10,700 to 8600 cal yr BP*

Magnetic parameters exhibit increased values during this period. In fact, they are the highest in the entire core. Values of χ_{lf} range from 116.26 to 150.59 × 10^{-8} m^3 kg^{-1} (average = 138.13 × 10^{-8} m^3 kg^{-1}), those of χ_{ARM} from 1.0 to 1.46 × 10^{-5} m^3 kg^{-1} (average = 1.3 × 10^{-5} m^3 kg^{-1}), and SIRM from 628.0 to 912.0 × 10^{-5} Am^2 kg^{-1} (average = 773.1 × 10^{-5} Am^2 kg^{-1}). There is also an increase in the concentration of SP grains (= higher pedogenesis) as evidenced by the high χ_{fd} (average = 15.8 × 10^{-8} m^3 kg^{-1}) values. S-ratio exhibits slightly high and HIRM low values compared to the earlier period. A prominent peak in HIRM (a trough in S-ratio) values is documented at ~9997 cal yr BP.

The carbonate content is profoundly low with values ranging from 0.01 to 0.18%. The average C_{org} and N contents are 1.26% and 0.13% respectively with sharp peaks around 9800 cal yr BP. The C_{org}/N ratio range from 10.1 to 15.8, indicating an increased contribution from aquatic plants. There is a shift in the source of organic matter from essentially terrestrial (without any planktonic contribution) in the earlier period to a mixed (planktonic + terrestrial) vegetation during this period. Except one sample (which has a depleted $\delta^{13}C$ value of −24.8‰), the others exhibit much enriched values of −16.6 and −17.9‰ (Scenario 2). The $\delta^{13}C$ values of −16.6 and −17.9‰ indicate an increased contribution from C4 land plants. A value of −24.8‰, on the other hand, indicates a higher contribution from C3 land plants, indicating a higher rainfall.

The data presented above suggest that this period is characterized by relatively high rainfall compared to the Present; in fact, it is the highest for the entire Holocene. Thus, it may represent the Early Holocene Optimum (Ciais et al., 1992; Bookhagen et al., 2006).

III. *~8600 to 4500 cal yr BP*

This period is characterized by notably low values for the parameters, χ_{lf}, χ_{ARM} and SIRM except for two prominent peaks. The values of χ_{lf} range from 88 to 128 × 10^{-8} m^3 kg^{-1} (average = 103.4 × 10^{-8} m^3 kg^{-1}), those of χ_{ARM} from 0.7 to 1.2 × 10^{-5} m^3 kg^{-1} (average = 0.93 × 10^{-5} m^3 kg^{-1}) and SIRM from 476.5 to 739.0 × 10^{-5} Am^2 kg^{-1} (average = 559.7 × 10^{-5} Am^2 kg^{-1}).

The carbonate content ranges from 0.09 to 1.6%. The average C_{org} content is 1.02% and the average N content 0.07%. The C_{org}/N ratio varies from 10.1 to 23.9 (average = 17.8), which indicates a mixed (both planktonic and terrestrial) origin of organic matter. But around 5600 and 7800 cal yr BP, the C_{org}/N ratio exhibits values >20 (23.9 and 22.3) even though the values are not as high as for the Early Holocene, suggesting a significant reduction in plankton. Carbon isotopic values range from −15.9 to −18.9‰, indicating an increased contribution from C4 plants (Scenario 1). Hence, the lake had not dried up fully even under arid conditions as evidenced by the average C_{org}/N value of 17.8.

On the basis of the data discussed above, this period appears to be characterized by low rainfall/arid climatic conditions. It may correspond to the period of Mid-Holocene aridity documented in some palaeomonsoonal records (Bryson and Swain, 1981; Sukumar et al., 1993).

IV. *~4500 to 3300 cal yr BP*

The concentration-dependent parameters exhibit rapid fluctuations during this period. The χ_{lf} values range from 65.5–137.3 × 10^{-8} m^3 kg^{-1}, χ_{ARM} values from 0.5 to 1.1 × 10^{-5} m^3 kg^{-1} and SIRM values from 332.8 to 846.9 × 10^{-5} Am^2 kg^{-1}. A major peak in these parameters is discernible at ~4300 cal yr BP after which there is a rapid decline, with the lowest value recorded at ~3600 cal yr BP. Thereafter, the parameters again register a rapid increase up to 3300 cal yr BP. The χ_{fd} values also exhibit a similar trend of rapid fluctuations.

The C_{org}/N ratio registers an increase in the value from 9.1 to 36.3, suggesting a steady change from plankton-dominated deep water conditions to fully terrestrial (total absence of aquatics) vegetation. The C_{org}/N ratio is probably indicative of drying up of the lake. But the carbonate content (1.5 to 1.8%) and $\delta^{13}C$ values (−16.6 to −17.7‰) vary only a little. A value of −17.7‰ is due to higher contributions from C4 plants (because the C_{org}/N ratio is significantly high; fully terrestrial and total absence of aquatics). The C_{org} content does not exhibit any rapid fluctuations whereas N content exhibits a decrease (0.13–0.05%).

Considering the foregoing data, this period appears to be a short interval of fluctuating monsoonal conditions. The monsoon intensity was strong in the beginning of this period, but subsequently waned to its minimum and increased thereafter.

V. *~3300 cal yr BP to the Present*

After ~3300 cal yr BP, χ_{lf}, χ_{ARM}, SIRM values are constant. The values are high but not as high as those recorded during the Early Holocene. The average χ_{lf}, χ_{ARM}, SIRM values are 114.8 × 10^{-8} m^3 kg^{-1}, 0.97 × 10^{-5} m^3 kg^{-1} and 586.9 × 10^{-5} Am^2 kg^{-1} respectively. The lowest values (not only for this but the entire period represented by the core) are documented at ~1028 cal yr BP (χ_{lf} = 32.8 × 10^{-8} m^3 kg^{-1}; χ_{ARM} = 0.15 × 10^{-5} m^3 kg^{-1} and SIRM = 126.6 × 10^{-5} Am^2 kg^{-1} respectively). The χ_{fd} values also exhibit a similar trend.

Excluding one sample with a markedly high C_{org}/N ratio value, the average values are relatively low (9.9–18.7; average = 13.3; Scenario 2), indicating a mixed vegetation. The anomalous sample also has an enriched $\delta^{13}C$ value (−17.5‰). The $\delta^{13}C$ values display a decreasing trend towards the Present (−18 to −20.9‰; average = −18.9‰) which points to an increasing contribution from C3 land plants.

The data presented above indicate that the monsoon has been steady from 3300 cal yr BP to the Present.

5.5. Comparison with other palaeoclimatic records from the region

Fig. 8 illustrates the correspondence between the magnetic susceptibility data of SS-1 and palaeoclimatic records from different proxies. The weak monsoonal conditions documented in the SS-1 record prior to ~10,700 cal yr BP, *i.e.*, before the dawn of the Holocene (the Younger Dryas) is also reported by several investigators (Tiwari et al., 2006; Altabet et al., 2002 and references therein). Staubwasser et al. (2003) documented a reduced discharge from the Sindhu (Indus) River during the Younger Dryas.

Strong monsoonal conditions are indicated by the SS-1 record during ~10,700–8600 cal yr BP, coinciding with the increased insolation then (14°N latitude, June 21; Laskar, 1990). Thamban et al. (2007) also reported peak monsoonal conditions between 9500 and 8000 cal yr BP based on proxies like magnetic susceptibility and elemental concentrations of a sediment core collected from the western continental margin of India. A maximum in the Sindhu River discharge off the Pakistan coast and thermocline anoxia were established in the Arabian Sea during this period (Staubwasser et al., 2002, 2003). Based on the denitrification intensity (which is closely related to the SW monsoon wind strength) recorded in sediment cores from the Oman margin, Altabet et al. (2002) documented an increased productivity during this period. This Early Holocene precipitation maximum is also recorded in the speleothem records from northern Oman (Neff et al., 2001) and marine sediments off Oman (Gupta et al., 2003). Thamban et al.'s (2007) study also revealed intensification of monsoon during the Early Holocene that occurred in two abrupt steps at 9400 and 9100 years BP, with the main event between 9100 and 8500 years BP. The SS-1 record also shows that the monsoon intensified abruptly but the intensification started slightly earlier at ~10,760 cal yr BP. But this Early Holocene high rainfall interval ended synchronously according to both the records; besides, the ending was gradual and not abrupt like the intensification event. A sudden decrease in the Sindhu discharge at 8400 cal yr BP in

the NE Arabian Sea was also documented (Staubwasser et al., 2002). The trend towards aridity began around the same time as per the SS-1 record as well. The Early Holocene monsoon intensification is also evident in recent records from lacustrine (Sarkar et al., 2015; Rawat et al., 2015a, 2015b) and marine (Kessarkar et al., 2013; Saraswat et al., 2016) sediments.

Fleitmann et al. (2003) and Gupta et al. (2003, 2005) documented a declining trend in the Indian monsoon precipitation up to 1.5 ka after the maximum at ~8.5 ka. They also proposed that the monsoon trend broadly followed the insolation curve at 65°N. Sarkar et al. (2000), based on oxygen and carbon isotopic analyses of planktonic foraminifera, inferred that the monsoon decreased steadily from 10 ka to ~2 ka. But such a continuous decreasing trend is not documented in the SS-1 as well as other palaeoclimatic records from the region although the Early Holocene high precipitation event is discernible in all of them. In fact, the SS-1 record shows fluctuating monsoonal conditions during the Holocene with abrupt intervals of strong and weak monsoon. On the contrary, Bhushan et al. (2001) and Agnihotri et al. (2003), based on palaeoproductivity proxies ($CaCO_3$ and C_{org}) and denitrification intensity documented respectively in sediment cores from the eastern Arabian Sea, reported increasing SW monsoon intensity from ~10 to 2 ka.

The ~8600 to 4500 cal yr BP period is characterized by a particularly weak monsoon in the SS-1 record. Insolation also exhibited a decreasing trend during this period. Archaeological and other continental records from the Indian sub-continent depict a substantial weakening of the summer monsoon around 7000 cal yr BP (Gupta et al., 2006). However, a small peak in monsoon is shown by the SS-1 record during this time and a low rainfall recorded slightly earlier (~7800 cal yr BP). But except for two smaller peaks, rainfall was profoundly low during this period as per the SS-1 record. Thamban et al. (2007) documented a significantly weak monsoon between 6000 and 5500 cal yr BP. A decreased productivity was documented in the Oman margin (Gupta et al., 2005) during the same period. Saraswat et al. (2016) documented a distinct shift in evaporation-precipitation at 6400 cal yr BP accompanied by a cooling in the SST, which was evident in the low primary productivity in the eastern Arabian Sea. This event is not only recorded in marine sediments but also in the lacustrine sediments of Central India (Lonar Lake; Sarkar et al., 2015) and the Himalaya (Rawat et al., 2015a, 2015b). It is noteworthy that insolation reached minimal values around this time, after which it was steady albeit with a gentle increasing trend.

6. Conclusions

The present study of environmental magnetism, sedimentology, organic geochemistry and carbon isotopes besides geochronology of SS-1 core sediments from Shantisagara Lake provides palaeomonsoonal/palaeovegetational record of southern India for the Holocene Period. The following conclusions may be drawn from the present study:

- The 11,100-year palaeoclimatic record provided by SS-1 core of Shantisagara is the longest reported from any lake in Peninsular India.
- Periods of high rainfall are characterized by high values of concentration-dependent magnetic parameters like χ_{lf}, χ_{fd}, χ_{ARM} and SIRM, high sand content, low C_{org}/N ratio (fully aquatic-deep water conditions), more depleted $\delta^{13}C$ values (more C3 terrestrial plants). Periods of low rainfall, on the contrary, are typified by low values of concentration-dependent magnetic parameters (χ_{lf}, χ_{fd}, χ_{ARM} and SIRM), high clay content, high C_{org}/N ratio (total absence of aquatics; dried up lake), and less negative $\delta^{13}C$ values (more C4 terrestrial plants).
- The Indian summer monsoon (ISM) was significantly weak over southern India before the advent of the Holocene Period, i.e., 11,100–10,700 cal yr BP. This period may represent the end stage of the Younger Dryas cold event.
- The Early Holocene Period (10,700 to 8600 cal yr BP) was characterized by intensified ISM. During this period isolation was also the

highest, which might have led to intensification of monsoon.
- The ISM weakened during the 8600–4500 cal yr BP period (Mid-Holocene). This period corresponds to the Mid-Holocene aridity event documented in some palaeomonsoonal records; the sudden weakening of ISM around 8200 cal yr BP corresponds to the 8.2 ka cold event. Insolation exhibits a decreasing trend during this period.
- The 4500 to 3300 cal yr BP period witnessed fluctuating monsoonal conditions. From 4500 cal yr BP onwards the monsoon began to weaken, corresponding to the 4.2 ka cold aridity event. After waning to its minimum, ISM regained the earlier intensity.
- The monsoon has been steady from 3300 cal yr BP to the Present.
- There are similarities between many palaeomonsoonal records from the region and the SS-1 record, which indicate that Shantisagara sediments were able to record not only the local, but regional climatic variations as well.

Acknowledgements

References

Agnihotri, R., Bhattacharya, S.K., Sarin, M.M., Somayajulu, B.L.K., 2003. Changes in the surface productivity and subsurface denitrification during the Holocene: a multi proxy study from the eastern Arabian Sea. The Holocene 13, 701–713.

Altabet, M.A., Higginson, M.J., Murray, D.W., 2002. The effect of millennial changes in Arabian Sea dentitrification on atmospheric CO2. Nature 415, 159–162.

Anderson, N.J., Rippey, B., 1988. Diagenesis of magnetic minerals in the recent sediments of a eutrophic lake. Limnol. Oceanogr. 33, 1476–1492.

Bhattacharyya, A., Sandeep, K., Misra, S., Shankar, R., Warrier, A.K., Weijian, Z., Zuefeng, L., 2015. Vegetational and climatic variations during the past 3100 years in southern India: evidence from pollen, magnetic susceptibility and particle size data. Environ. Earth Sci. 74, 3559–3572.

Bhushan, R., Dutta, K., Somayajulu, B.L.K., 2001. Concentrations and burial fluxes of organic and inorganic carbon on the eastern margins of the Arabian Sea. Mar. Geol. 178, 95–113.

Blaauw, M., 2010. Methods and code for 'classical' age-modelling of radiocarbon sequences. Quat. Geochronol. 5, 512–518.

Bloemendal, J., King, J.W., Hall, F.R., Doh, S.-J., 1992. Rock magnetism of Late Neogene and Pleistocene deep-sea sediments: relationship to sediment source, diagenetic processes, and sediment lithology. J. Geophys. Res. 97 (B4), 4361–4375.

Bloemendal, J., Ehrmann, W., Hambrey, M.J., McKelvey, B.C., Matthews, R., Whitehead, J.M., 2003. Geochemical and rock magnetic records from sediments of the Cenozoic Pagodroma Group, Prince Charles Mountains, East Antarctica: implications for provenance and weathering. Antarct. Sci. 15 (3), 365–378.

Bookhagen, B., Fleitmann, D., Nishiizumi, K., Strecker, M.R., Thiede, R.C., 2006. Holocene monsoonal dynamics and fluvial terrace formation in the northwest Himalaya, India. Geology 34 (7), 601–604.

Borgaonkar, H.P., Sikder, A.B., Ram, S., Pant, G.B., 2010. El Niño and related monsoon drought signals in 523-year-long ring width records of teak (Tectona grandis L.F.) trees from south India. Palaeogeogr. Palaeoclimatol. Palaeoecol. 285, 74–84.

Bryson, R.A., Swain, A.M., 1981. Holocene variations in monsoon rainfall in Rajasthan. Quat. Res. 16, 135–145.

Carver, R.E., 1971. Procedures in Sedimentary Petrology. Wiley-Interscience, John Wiley and Sons Inc. (653 p.).

Chen, J., Wan, G., Wang, F., Zhang, D.D., Huang, R., Zhang, F., Schmidt, R., 2002. Environmental records of carbon in recent lake sediments. Sci. China. Ser. D Earth Sci. 45 (10), 875–884.

Chen, J., Wan, G., Zhang, D.D., Zhang, F., Huang, R., 2004. Environmental records of lacustrine sediments in different time scales: sediment grain size as an example. Sci. China. Ser. D Earth Sci. 47 (10), 954–960.

Church, J., White, N., 2006. A 20th century acceleration in global sea-level rise. Geophys. Res. Lett. 33:L01602. http://dx.doi.org/10.1029/2005GL024826.

Ciais, P., Petit, J.R., Jouzel, J., Lorius, C., Barkov, N.I., Lipenkov, V., Nicolaiev, V., 1992. Evidence for an early Holocene climatic optimum in the Antarctic deep ice-core record. Clim. Dyn. 6, 169–177.

Conroy, J.L., Overpeck, J.T., Cole, J.E., Shanahan, T.M., Steinitz-Kannan, 2008. Holocene changes in eastern tropical Pacific climate inferred from a Galápagos lake sediment record. Quat. Sci. Rev. 27, 1166–1180.

Dansgaard, W., Johnsen, S.J., Clausen, H.B., Dahljensen, D., Gundestrup, N.S., Hammer, C.U., Hvidberg, C.S., Steffensen, J.P., Sveinbjörnsdóttir, A.E., Jouzel, J., Bond, G., 1993. Evidence for general instability of past climate from a 250-kyr ice-core record. Nature 364 (6434), 218–220.

Dearing, J.A., 1999a. Magnetic susceptibility. In: Walden, J., Smith, J.P., Oldfield, F. (Eds.), Environmental Magnetism - A practical guide. Technical Guide No. 6. Quaternary Research Association, London, pp. 35–62.

Dearing, J.A., 1999b. Holocene environmental change from magnetic proxies in lake sediments. In: Maher, B.A., Thompson, R. (Eds.), Quaternary Climates, Environments and Magnetism. Cambridge University Press, Cambridge, pp. 231–278.

Dearing, J.A., Hay, K.L., Baban, S.M.J., Huddleston, A.S., Wellington, E.M.H., Loveland, P.J., 1996. Magnetic susceptibility of soil: an evaluation of conflicting theories using a national data set. Geophys. J. Int. 127, 728–734.

Dearing, J.A., Bird, P.M., Dann, R.J.L., Benjamin, S.F., 1997. Secondary ferromagnetic minerals in Welsh soils: a comparison of mineral magnetic detection methods and implications for mineral formation. Geophys. J. Int. 130, 727–736.

Demske, D., Tarasov, P.E., Wünnemann, B., Riedel, F., 2009. Late glacial and Holocene vegetation, Indian monsoon and westerly circulation dynamics in the Trans-Himalaya recorded in the pollen profile from high-altitude Tso Kar Lake, Ladakh, NW India. Palaeogeogr. Palaeoclimatol. Palaeoecol. 279 (3), 172–185.

Dixit, Y., Hodell, D.A., Sinha, R., Petrie, C.A., 2014a. Abrupt weakening of the Indian summer monsoon at 8.2 kyrBP. Earth Planet. Sci. Lett. 391, 16–23.

Dixit, Y., Hodell, D.A., Petrie, C.A., 2014b. Abrupt weakening of the summer monsoon in northwest India ~4100 yr ago. Geology 42 (4), 339–342.

Dykoski, C.A., Edwards, R.L., Cheng, H., Yuan, D., Cai, Y., Zhang, M., Lin, Y., Qing, J., An, Z., Revenaugh, J., 2005. A high-resolution absolute-dated Holocene and deglacial Asian monsoon record from Dongge Cave, China. Earth Planet. Sci. Lett. 233, 71–86.

Evans, M.E., Heller, F., 2003. Environmental Magnetism. Principles and Applications of Enviromagnetics. Academic Press, San Diego, USA (299 p).

Fleitmann, D., Burns, S.J., Mudelsee, M., Neff, U., Kramers, J., Mangini, A., Matter, A., 2003. Holocene forcing of the Indian monsoon recorded in a stalagmite from Southern Oman. Science 300, 1737–1739.

Fleitmann, D., Burns, S.J., Mangini, A., Mudelseed, M., Kramers, J., Villa, I., Neffe, U., Al-Subbary, A.A., Buettner, A., Hippler, D., Matter, A., 2007. Holocene ITCZ and Indian monsoon dynamics recorded in stalagmites from Oman and Yemen (Socotra). Quat. Sci. Rev. 26, 170–188.

Gautam, P., Blaha, U., Appel, E., Neupane, G., 2004. Environmental magnetic approach towards the quantification of pollution in Kathmandu urban area, Nepal. Phys. Chem. Earth 29, 973–984.

Geological and Mineral Map of Karnataka and Goa, 1981. Geological Survey of India, Scale 1: 500,000, 1 Sheet (Compiled by: Swaminath, J., Ramiengar, A.S., Ziauddin, M., Narayanamurthy, J., Seshadri, T.S., Ramakrishnan, M., Viswanatha, M.N. and Murthy, T.S.S).

Grootes, P.M., Stuvier, M., White, J.W.C., Johnsen, S.J., Jouzel, J., 1993. Comparison of oxygen isotope records from GISP2 and GRIP Greenland ice cores. Nature 366, 552–554.

Gupta, A.K., Anderson, D.M., Overpeck, J.T., 2003. Abrupt changes in the Asian southwest monsoon during the Holocene and their links to the North Atlantic Ocean. Nature 421, 354–357.

Gupta, A.K., Das, M., Anderson, D.M., 2005. Solar influence on the Indian summer monsoon during the Holocene. Geophys. Res. Lett. 32. http://dx.doi.org/10.1029/2005GL022685.

Gupta, A.K., Anderson, D.M., Pandey, D.N., Singhvi, A.K., 2006. Adaptation and human migration, and evidence of agriculture coincident with changes in the Indian summer monsoon the Holocene. Curr. Sci. 90, 1082–1090.

Heslop, D., 2009. On the statistical analysis of the rock magnetic S-ratio. Geophys. J. Int. 178, 159–161.

India Meteorological Department, 2008. Rainfall data for Chennagiri Station. Government of India, New Delhi.

Karnataka Forest Department, 2003. Working Plan for the Forests of Bhadravathi Division. Aranya Bhavan, Government of Karnataka, Bangalore.

Kessarkar, K.M., Rao, V.P., Naqvi, S.W.A., Karapurkar, S.G., 2013. Variation in the Indian Summer Monsoon intensity during the Bølling-Ållerød and Holocene. Paleoceanography 28 (3), 413–425.

King, J.W., Banerjee, S.K., Marvin, J., Õzdemir, Õ., 1982. A comparison of different magnetic methods for determining the relative grain size of magnetite in natural materials: some results from lake sediments. Earth Planet. Sci. Lett. 59, 404–419.

Lamb, A.L., Wilson, G.P., Leng, M.J., 2006. A review of coastal palaeoclimate and relative sea-level reconstructions using $\delta^{13}C$ and C/N ratios in organic material. Earth Sci. Rev. 75 (1–4), 29–57.

Laskar, J., 1990. The chaotic motion of the solar system: a numerical estimate of the size of the chaotic zones. Icarus 88, 266–291.

Lowe, J.J., Walker, M.J.C., 2014. Reconstructing Quaternary Environments. third ed. Routledge, London.

Maher, B.A., 1988. Magnetic properties of some synthetic sub-micron magnetites. Geophys. J. 94, 83–96.

Maher, B.A., Taylor, R.M., 1988. Formation of ultrafine-grained magnetite in soils. Nature 336, 368–370.

Maher, B.A., Thompson, R., 1992. Paleoclimatic significance of the mineral magnetic record of the Chinese loess and paleosols. Quat. Res. 39, 155–170.

Maher, B.A., Thompson, R., Hounslow, M.W., 1999. Quaternary Climates, Environments and Magnetism. Cambridge University Press, Cambridge.

Mayewski, P.A., Rohling, E.E., Stager, J.C., Karlen, W., Maasch, K.A., Meeker, L.D., Meyerson, E.A., Gasse, F., van Kreveld, S., Holmgren, K., Lee-Thorp, J., Rosqvist, G., Rack, F.,

Staubwasser, M., Schneider, R.R., Steig, E.J., 2004. Holocene climate variability. Quat. Res. 62, 243–255.

Meyers, P.A., 2003. Applications of organic geochemistry to paleolimnological reconstructions: a summary of examples from the Laurentian Great Lakes. Org. Geochem. 34, 261–289.

Meyers, P.A., Ishiwatari, R., 1993. Lacustrine organic geochemistry - an overview of indicators of organic matter sources and diagenesis in lake sediments. Org. Geochem. 20, 867–900.

Meyers, P.A., Lallier-Verges, E., 1999. Lacustrine sedimentary organic matter records of Late Quaternary paleoclimates. J. Paleolimnol. 21, 345–372.

Meyers, P.A., Terranes, J.L., 2001. Sediment organic matter. In: Last, W.M., Smol, J.P. (Eds.), Tracking Environmental Change Using Lake Sediments. Volume 2: Physical and Geochemical Methods. Kluwer Academic Publishers, Dordrecht, Netherlands.

Mishra, P.K., Prasad, S., Anoop, A., Plessen, B., Jehangir, A., Gaye, B., Menzel, P., Weise, S.M., Yousuf, A.R., 2015. Carbonate isotopes from high altitude Tso Moriri Lake (NW Himalayas) provide clues to late glacial and Holocene moisture source and atmospheric circulation changes. Palaeogeogr. Palaeoclimatol. Palaeoecol. 425, 76–83.

Naik, S.S., Godad, S.P., Naidu, P.D., Tiwari, M., Paropkari, A.L., 2014. Early- to late- Holocene contrast in productivity, OMZ intensity and calcite dissolution in the eastern Arabian Sea. The Holocene 24, 749–755.

Neff, U., Burns, S.J., Mudelsee, M., Mangini, A., Matter, A., 2001. Strong coherence between solar variability and the monsoon in Oman between 9 and 6 kyrs ago. Nature 411, 290–293.

Nigam, R., Khare, N., Nair, R.R., 1995. Foraminiferal evidences for 77 years cycle of drought in India and its possible modulation by the Gleissberg solar cycle. J. Coast. Res. 11, 1099–1107.

Northfelt, D.W., DeNiro, M.J., Epstein, S., 1981. Hydrogen and carbon isotopic ratios of the cellulose nitrate and saponifiable lipid fractions prepared from annual growth rings of a California redwood. Geochim. Cosmochim. Acta 45, 1895–1898.

Oldfield, F., 1991. Environmental magnetism - a personal perspective. Quat. Sci. Rev. 10, 73–85.

Oldfield, F., 1994. Toward the discrimination of fine grained ferrimagnets by magnetic measurements in lake and near-shore marine sediments. J. Geophys. Res. 99, 9045–9050.

Oldfield, F., 2007. Sources of fine grained magnetic minerals in sediments: a problem revisited. The Holocene 17 (8), 1265–1271.

Oldfield, F., Crowther, J., 2007. Establishing fire incidence in temperate soils using magnetic measurements. Palaeogeogr. Palaeoclimatol. Palaeoecol. 249, 362–369.

Prasad, S., Anoop, A., Riedel, N., Sarkar, S., Menzel, P., Basavaiah, N., Krishnan, R., Fuller, D., Plessen, B., Gaye, B., Röhl, U., Wilkes, H., Sachse, D., Sawant, R., Wiesner, M.G., Stebich, M., 2014. Prolonged monsoon droughts and links to Indo-Pacific warm pool: a Holocene record from Lonar Lake, central India. Earth Planet. Sci. Lett. 391, 171–182.

R Development Core Team, 2013. R: A Language and Environment for Statistical Computing. R Foundation for Statistical Computing, Vienna, Austria 3-900051-07-0 http://www.r-project.org.

Radhakrishna, B.P., Vaidyanadhan, R.V., 1994. Geology of Karnataka. Geological Society of India, Bangalore.

Rawat, S., Gupta, A.K., Srivastava, P., Sangode, S.J., Nainwal, H.C., 2015a. A 13,000 year record of environmental magnetic variations in the lake and peat deposits from the Chandra valley, Lahaul: implications to Holocene monsoonal variability in the NW Himalaya. Palaeogeogr. Palaeoclimatol. Palaeoecol. 440, 116–127.

Rawat, S., Gupta, A.K., Sangode, S.J., Srivastava, P., Nainwal, H.C., 2015b. Late Pleistocene–Holocene vegetation and Indian summer monsoon record from the Lahaul, Northwest Himalaya, India. Quat. Sci. Rev. 114, 167–181.

Reimer, P.J., Bard, E., Bayliss, A., Beck, J.W., Blackwell, P.G., Bronk Ramsey, C., Buck, C.E., Edwards, R.L., Friedrich, M., Grootes, P.M., Guilderson, T.P., Haflidason, H., Hajdas, I., Hatté, C., Heaton, T.J., Hoffmann, D.L., Hogg, A.G., Hughen, K.A., Kaiser, K.F., Kromer, B., Manning, S.W., Niu, M., Reimer, R.W., Richards, D.A., Scott, E.M., Southon, J.R., Turney, C.S.M., van der Plicht, J., 2013. IntCal13 and Marine13 radiocarbon age calibration curves, 0-50,000 years cal BP. Radiocarbon 55, 1869–1887.

Roxy, M.K., Modi, A., Murutugudde, R., Valsala, V., Panickal, S., Prasanna Kumar, S., Ravichandran, M., Vichi, M., Levy, M., 2016. A reduction in marine primary productivity driven by rapid warming over the tropical Indian Ocean. Geophys. Res. Lett. 43, 826–833.

Rühland, K., Jacques, J.M., Beierle, B.D., Lamoureux, S.F., Dyke, A.S., John, P., 2009. Lateglacial and Holocene paleoenvironmental changes recorded in lake sediments, Brock Plateau (Melville Hills), Northwest Territories, Canada. The Holocene 19 (7), 1005–1016.

Sandeep, K., Warrier, A.K., Harshavardhana, B.G., Shankar, R., 2012. Rock magnetic investigations of surface and sub-surface soil samples from five lake catchments in tropical Southern India. Int. J. Environ. Res. 6 (1), 1–18.

Sandeep, K., Shankar, R., Warrier, A.K., Weijian, Z., Xuefeng, L., 2015. The environmental magnetic record of palaeoenvironmental variations during the past 3100 years: a possible solar influence? J. Appl. Geophys. 118, 24–36.

Sandeep, K., Shankar, R., Warrier, A.K., Balsam, W., 2017. Diffuse Reflectance Spectroscopy of a tropical southern Indian lake sediment core: A window to environmental change. Episodes 40 (1), 47–56.

Saraswat, R., Lea, D.W., Nigam, R., Mackensen, A., Naik, D.K., 2013. Deglaciation in the tropical Indian Ocean driven by interplay between the regional monsoon and global teleconnections. Earth Planet. Sci. Lett. 375, 166–175.

Saraswat, R., Naik, D.K., Nigam, R., Gaur, A.S., 2016. Timing, cause and consequences of mid-Holocene climate transition in the Arabian Sea. Quat. Res. 86 (2), 162–169.

Sarkar, A., Ramesh, R., Somayajulu, B.L.K., Agnihotri, R., Jull, A.J.T., Burr, G.S., 2000. High resolution Holocene monsoon record from the eastern Arabian Sea. Earth Planet. Sci. Lett. 177, 209–218.

Sarkar, S., Prasad, S., Wilkes, H., Riedel, N., Stebich, M., Basavaiah, N., Sachse, D., 2015. Monsoon source shifts during the drying mid-Holocene: biomarker isotope based evidence from the core 'monsoon zone' (CMZ) of India. Quat. Sci. Rev. 123, 144–157.

Schumacher, B.A., 2002. Methods for the Determination of Total Organic Carbon (TOC) in Soils and Sediments. Ecological Risk Assessment Support Center, Office of Research and Development, US. Environmental Protection Agency (23 p).

Shankar, R., Prabhu, C.N., Warrier, A.K., Vijayakumar, G.T., Sekar, B., 2006. A multi-decadal rock magnetic record of monsoonal variations during the past 3,700 years from a tropical Indian tank. J. Geol. Soc. India 68 (3), 447–459.

Snowball, I., 1991. Magnetic hysteresis properties of greigite (Fe$_3$S$_4$) and a new occurrence in Holocene sediments from Swedish Lappland. Phys. Earth Planet. Inter. 68, 32–40.

Snowball, I., 1994. Bacterial magnetite and the magnetic properties of sediments in a Swedish lake. Earth Planet. Sci. Lett. 126, 129–142.

Staubwasser, M., Sirocko, F., Grootes, P.M., Erlenkeuser, H., 2002. South Asian monsoon climate change and radiocarbon in the Arabian Sea during early and mid Holocene. Paleoceanography 17:1063. http://dx.doi.org/10.1029/2000PA000608.

Staubwasser, M., Sirocko, F., Grootes, P.M., Segl, M., 2003. Climate change at the 4.2 ka BP termination of the Indus valley civilization and Holocene south Asian monsoon variability. Geophys. Res. Lett. 30:1425. http://dx.doi.org/10.1029/2002GL016822.

Sukumar, R., Ramesh, R., Pant, R.K., Rajagopalan, G., 1993. A δ^{13}C record of late Quaternary climate change from tropical peats in southern India. Nature 364, 703–706.

Thamban, M., Kawahata, H., Rao, V.P., 2007. Indian summer monsoon variability during the Holocene as recorded in sediments of the Arabian Sea: timing and implications. J. Oceanogr. 63, 1009–1020.

Thompson, R., Oldfield, F., 1986. Environmental Magnetism. Allen & Unwin, London (227 p).

Tiwari, M., Ramesh, R., Somayajulu, B.L.K., Jull, A.J.T., Burr, G.S., 2006. Paleomonsoon precipitation deduced from a sediment core from the equatorial Indian Ocean. Geo-Mar. Lett. 26, 23–30.

Walden, J., 1999. Remanence measurements. In: Walden, J., Smith, J.P., Oldfield, F. (Eds.), Environmental Magnetism - A Practical Guide, Technical Guide No. 6. Quaternary Research Association, London, pp. 63–88.

Walden, J.F., Oldfield, F., Smith, J., 1999. Environmental Magnetism: A Practical Guide, No.6. Quaternary Research Association, London (243 p).

Wanner, H., Beer, J., Bütikofer, J., Crowley, T.J., Cubasch, U., Fluckiger, J., Goosse, H., Grosjean, M., Joos, F., Kaplan, J.O., Küttel, M., Müller, S.A., Prentice, I.C., Solomina, O., Stocker, T.F., Tarasov, P., Wagner, M., Widmann, M., 2008. Mid- to Late Holocene climate change: an overview. Quat. Sci. Rev. 27, 1791–1828.

Wanner, H., Mercolli, L., Grosjean, M., Ritz, S.P., 2014. Holocene climate variability and change; a data-based review. J. Geol. Soc. 172, 254–263.

Warrier, A.K., Shankar, R., 2009. Geochemical evidence for the use of magnetic susceptibility as a paleorainfall proxy in the tropics. Chem. Geol. 265, 553–562.

Warrier, A.K., Shankar, R., Sandeep, K., 2014. Sedimentological and carbonate data evidence for lake level variations during the past 3700 years from a southern Indian lake. Palaeogeogr. Palaeoclimatol. Palaeoecol. 397, 52–60.

Warrier, A.K., Sandeep, K., Shankar, R., 2017. Climatic periodicities recorded in Lake sediment magnetic susceptibility data: further evidence for solar forcing on the Indian summer monsoon. Geoscience Frontiers. http://dx.doi.org/10.1016/j.gsf.2017.01.004.

Yadava, M.G., Ramesh, R., 1999. Speleothems - useful proxies for past monsoon rainfall. J. Sci. Ind. Res. 58, 339–348.

Yadava, M.G., Ramesh, R., Pant, G.B., 2004. Past monsoon rainfall variations in peninsular India recorded in a 331-year-old speleothem. The Holocene 14 (4), 517–524.